Geophysical Journal International

Geophys. J. Int. (2013) **192,** 861–870 doi: 10.1093/gji/ggs064

Crustal properties from seismic station autocorrelograms

A. Gorbatov,[1] E. Saygin[2] and B. L. N. Kennett[2]

[1] *Geoscience Australia, GPO Box* 378, *Canberra ACT* 2601, *Australia. E-mail: alexei.gorbatov@ga.gov.au*
[2] *Research School of Earth Sciences, The Australian National University, Canberra ACT* 0200, *Australia*

Accepted 2012 November 6. Received 2012 October 2; in original form 2012 May 30

SUMMARY

Stations on the Australian continent receive a rich mixture of continuous ground motion with ambient seismic noise from the surrounding oceans, and numerous small earthquakes in the earthquake belts to the north in Indonesia, and east in Tonga-Kermadec, as well as more distant source zones. The ground motion at a seismic station contains information about the structure in the vicinity of the site, and this can be exploited by applying an autocorrelation procedure to the continuous records. By creating stacked autocorrelograms of the ground motion at a single station, information on crust properties can be extracted in the form of a signal that includes the crustal reflection response convolved with the autocorrelation of the combined effect of source excitation and the instrument response. After applying suitable high-pass filtering, the reflection component can be extracted to reveal the most prominent reflectors in the lower crust, which often correspond to the reflection at the Moho. Because the reflection signal is stacked from arrivals from a wide range of slownesses, the reflection response is somewhat diffuse, but still sufficient to provide useful constraints on the local crust beneath a seismic station.

Continuous vertical component records from 223 stations (permanent and temporary) across the continent have been processed using autocorrelograms of running windows 6 hr long with subsequent stacking. A distinctive pulse with a time offset between 8 and 30 s from zero is found in the autocorrelation results, with frequency content between 1.5 and 4 Hz, suggesting *P*-wave multiples trapped in the crust. Synthetic modelling, with control of multiple phases, shows that a local p_mp phase can be recovered with the autocorrelation approach. This identification enables us to make out the depth to the most prominent crustal reflector across the continent. We obtain results that largely conform to those from previous studies using a combination of data from refraction, reflection profiles and receiver functions. This approach can be used for crustal property extraction using just vertical component records, and effective results can be obtained with temporary deployments of just a few months.

Key words: Time series analysis; Body waves; Theoretical seismology; Wave propagation; Australia.

1 INTRODUCTION

The seismic structure of the Australian crust and upper mantle has been studied in numerous works exploiting active seismic studies (e.g. Collins 1991; Kennett *et al.* 2011), receiver function inversions (e.g. Clitheroe *et al.* 2000; Kennett *et al.* 2011), tomography (e.g. Yoshizawa & Kennett 2004; Saygin & Kennett 2010, 2012) and gravity inversion (e.g. Aitken 2010). Relatively dense coverage of most of the continent by recently enhanced permanent network supplemented by extensive portable seismic experiments together with abundant seismicity from surrounding Sunda and Tonga-Kermadec arcs makes the Australian continent an excellent location for studies of the Earth's lithosphere (e.g. Kennett & Blewett 2012). The results of a wide range of studies suggest thicker and colder lithosphere in the Western part of Australia, and thinner and warmer lithosphere in the East of the continent, mirroring the main geological features. The cratons of western and central Australian comprise Archaean to Paleoproterozoic rocks and are surrounded by Proterozoic orogens. In contrast, the eastern part of the continent is characterized by a series of crustal blocks accreted to the continental margin during the assembly of Gondwana, ca. 450–350 Ma (Betts *et al.* 2002). Recent detailed studies of Australian Moho have been undertaken by Kennett *et al.* (2011) using receiver functions and interpretation of reflection and refraction surveys. Existing detailed data on crustal and upper mantle discontinuities can be used as a benchmark to verify capability of methods of Earth structure imaging.

The pioneering work of Weaver & Lobkis (2001a,b) in acoustics, and subsequently Shapiro & Campillo (2004) and Shapiro *et al.* (2005) in seismology demonstrated that the stacked cross-correlation of seismic traces registered by two different seismic receivers is equivalent to the Green's function of the Earth structure between them. Subsequently analysis of stacked cross-correlograms of seismic traces in terms of the group dispersion of the prominent surface wave component has become a standard procedure used in ambient seismic noise tomography. The novel idea was extended to body wave analysis (e.g. Roux *et al.* 2005; Draganov *et al.* 2006; Zhan *et al.* 2010; Ruigrok *et al.* 2011; Poli *et al.* 2012) and sophisticated methods using body waves to study samples in laboratory experiments or reflection data retrieval in exploration seismology (e.g. Gouédard *et al.* 2008; Wapenaar *et al.* 2011) surged.

As the distance between the pair of seismic stations decreases, the surface wave component loses its dominance and the body wave interaction with the structure between the stations increases in importance. In the limit as the two stations coalesce, the cross-correlogram becomes the autocorrelogram for a single station. Claerbout (1968) studied the acoustic waves on a layered structure with a free surface and demonstrated that the autocorrelogram for a vertically incident plane wave transmitted through the structure provided sufficient information to recover the reflection response of the medium, including free surface multiples. His results were extended by Frasier (1970) for the case of coupled *P-SV* plane waves incident at angles inclined to the vertical. Wapenaar *et al.* (2004) have extended the concepts to three-dimensionally varying structure for both acoustic and elastic media. Successful application of autocorrelation to observed seismic data to extract reflections from the Moho was reported by Tibuleac & von Seggern (2012).

In this paper, we explore the properties of the autocorrelogram at a single seismic station in the presence of an varying continuous ground motion from ambient noise and earthquakes, and show how the reflection response beneath the station can be recovered with the aid of a high-pass filter. Because the wavefield consists of a wide range of slowness components, some degree of blurring of the reflection response is inevitable, but the strongest reflectors can be recognized.

2 NATURE OF AUTOCORRELOGRAMS

The ground motion at a station is composed of many different wave arrivals, which can be described by an angular spectrum of wave components. Much of the ground vibrations will be in the form of surface waves at various frequencies that will travel past the station propagating close to horizontal. However, embedded in the ground motion will be arrivals that reach the station from below with transmission through the crustal structure.

We can represent this suite of transmitted arrivals in the form of a slowness integral in the frequency domain (see, e.g. Kennett 2001, ch. 16; 2002, ch. 28),

$$\mathbf{w}_0(\omega) = \int_{-p_c}^{p_c} \mathrm{d}p\, \bar{\mathbf{w}}_0(p,\omega) = \int_{-p_c}^{p_c} \mathrm{d}p\, S_I(p,\omega)\mathbf{Z}^T(p,\omega)\mathbf{C}_\mathrm{R}^T(p,\omega)\Phi(p,\omega), \quad (1)$$

where $\Phi(p,\omega)$ represents the phase propagation effects from the sources, $\mathbf{Z}(p,\omega)$ includes amplitude effects prior to arrival at the zone below the station and $S_I(p,\omega)$ the combined effects of excitation and the instrumental response for the varied slownesses of the arriving waves at the station from uncorrelated sources. $\mathbf{C}_\mathrm{R}(p,\omega)$ describes the effect of structure local to the station. The superscript $(^T)$ denotes the transpose of the various matrices. For simplicity, we have suppressed an azimuthal integral in (1).

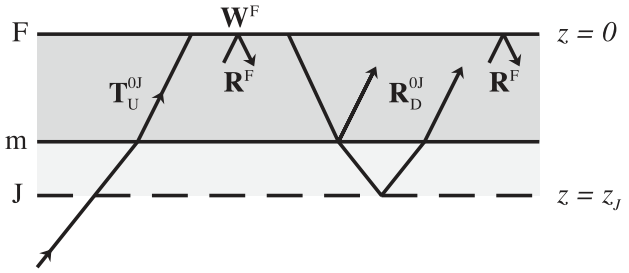

Figure 1. Representation of the transmission zone from level z_J to the surface. The lower boundary is taken below the base of the crust at *m*. The action of the transmission and reflection matrices is represented schematically.

We take a transmission zone from a level $z = z_J$ below the base of the crust to the surface at $z = 0$. The local structural term $\mathbf{C}_\mathrm{R}(p,\omega)$ can then be written as

$$\mathbf{C}_\mathrm{R}(p,\omega) = \mathbf{W}_\mathrm{F}(p)[\mathbf{I} - \mathbf{R}_\mathrm{D}^{0\mathrm{J}}(p,\omega)\mathbf{R}_\mathrm{F}(p)]^{-1}\mathbf{T}_\mathrm{U}^{0\mathrm{J}}(p,\omega), \quad (2)$$

in terms of the transmission matrix through the zone 0J: $\mathbf{T}_\mathrm{U}^{0\mathrm{J}}$, the reflection matrix at the free surface $\mathbf{R}_\mathrm{F}$, reflection back from 0J: $\mathbf{R}_\mathrm{D}^{0\mathrm{J}}$, and the amplification of ground motion at the free surface represented by $\mathbf{W}_\mathrm{F}$. $\mathbf{I}$ is the identity matrix. The relevant operators are represented schematically in Fig. 1.

For such transmitted arrivals, $\mathbf{W}_\mathrm{F}(p)$ is a slowly varying function of slowness p. The frequency dependence resides in the transmission $\mathbf{T}_\mathrm{U}^{0\mathrm{J}}(p,\omega)$ and in the surface generated reverberation through $\mathbf{R}_\mathrm{D}^{0\mathrm{J}}$. Working in terms of propagating waves normalized to unit energy transport in the vertical direction, we have general symmetry properties for reflection and transmission (Kennett *et al.* 1978)

$$\mathbf{R}_\mathrm{D}^{0\mathrm{J}} = [\mathbf{R}_\mathrm{D}^{0\mathrm{J}}]^T, \qquad \mathbf{T}_\mathrm{U}^{0\mathrm{J}} = [\mathbf{T}_\mathrm{D}^{0\mathrm{J}}]^T, \quad (3)$$

where the superscript $(^T)$ denotes a matrix transpose. For an isotropic reflection matrix, $\mathbf{R}_\mathrm{D}^{0\mathrm{J}}$ is block diagonal with a 2×2 matrix for *P-SV* waves and a single element for *SH* waves. The symmetry property (3) corresponds to symmetry in conversion *P-SV* and *SV-P*. In the case of anisotropy, the matrix is full, but the symmetry properties (3) still hold for the various components. For a perfectly elastic medium, we have a further property for propagating waves,

$$[\mathbf{R}_\mathrm{D}^{0\mathrm{J}}]^{T*}\mathbf{R}_\mathrm{D}^{0\mathrm{J}} + [\mathbf{T}_\mathrm{D}^{0\mathrm{J}}]^{T*}\mathbf{T}_\mathrm{D}^{0\mathrm{J}} = \mathbf{I}, \quad (4)$$

where the star denotes a complex conjugate. The spectral relation (4) corresponds to a direct link between the autocorrelograms of reflection and transmission processes.

We are particularly interested in the cases with a free surface, so we introduce the modified reflection and transmission matrices

$$\mathbf{T}_\mathrm{U}^{\mathrm{FJ}} = [\mathbf{I} - \mathbf{R}_\mathrm{D}^{0\mathrm{J}}\mathbf{R}_\mathrm{F}]^{-1}\mathbf{T}_\mathrm{U}^{0\mathrm{J}}, \qquad \mathbf{R}_\mathrm{D}^{\mathrm{FJ}} = [\mathbf{I} - \mathbf{R}_\mathrm{D}^{0\mathrm{J}}\mathbf{R}_\mathrm{F}]^{-1}\mathbf{R}_\mathrm{D}^{0\mathrm{J}}, \quad (5)$$

so that we can write

$$\mathbf{C}_\mathrm{R}(p,\omega) = \mathbf{W}_\mathrm{F}(p)\mathbf{T}_\mathrm{U}^{\mathrm{FJ}}(p,\omega). \quad (6)$$

The symmetry properties (3) extend to these modified terms so that, e.g. $\mathbf{T}_\mathrm{U}^{\mathrm{FJ}} = [\mathbf{T}_\mathrm{D}^{\mathrm{FJ}}]^T$. For a perfectly elastic medium, we have the property

$$\mathbf{I} + \mathbf{R}_\mathrm{F}(p)[\mathbf{R}_\mathrm{D}^{\mathrm{FJ}}(p,\omega)]^* + [\mathbf{R}_\mathrm{D}^{\mathrm{FJ}}(p,\omega)]^T[\mathbf{R}_\mathrm{F}(p)]^T = [\mathbf{T}_\mathrm{U}^{\mathrm{FJ}}(p,\omega)]^*[\mathbf{T}_\mathrm{U}^{\mathrm{FJ}}(p,\omega)]^T, \quad (7)$$

where the transmission symmetry has been employed to represent the right-hand side in terms of upward transmission. Frasier (1970)

was the first to obtain a relation equivalent to (7) for the *P-SV* system, and a convenient derivation is provided by Ursin (1983). Recognizing that the Fourier transform of a spectrum is the corresponding autocorrelogram, we see that (7) implies that the autocorrelation of the transmission response yields the combination of forward and reversed time reflection response. This relation, in the time domain, was recognized for purely vertically travelling waves by Kunetz & d'Erceville (1962) and Claerbout (1968), but we see that it has a much broader validity for purely propagating waves in transmission.An extension to 3-D varying media has been provided by Wapenaar *et al.* (2004). For a weakly attenuative medium, we can envisage that (7) will remain a reasonable approximation, but cannot be exact.

We note that the right-hand side of (7) is closely related to $\mathbf{C}_{\mathrm{R}}$. Indeed, we only need an extra factor of $\mathbf{W}_{\mathrm{F}}$ applied to $\mathbf{T}_{\mathrm{U}}^{\mathrm{FJ}}$; thus, we find

$$[\mathbf{C}_{\mathrm{R}}(p,\omega)]^{T*}\mathbf{C}_{\mathrm{R}}(p,\omega) = [\mathbf{W}_{\mathrm{F}}(p)]^{*}[\mathbf{W}_{\mathrm{F}}(p)]^{T} + [\mathbf{W}_{\mathrm{F}}(p)]^{*}(\mathbf{R}_{\mathrm{F}}(p)[\mathbf{R}_{\mathrm{D}}^{\mathrm{FJ}}(p,\omega)]^{*} + [\mathbf{R}_{\mathrm{D}}^{\mathrm{FJ}}(p,\omega)]^{T}[\mathbf{R}_{\mathrm{F}}(p)]^{T})[\mathbf{W}_{\mathrm{F}}(p)]^{T}, \quad (8)$$

since $\mathbf{R}_{\mathrm{F}}$ is symmetric, a further slight simplification is possible.

Let us now consider the autocorrelation of a single slowness component of the surface response by working in the frequency domain

$$[\bar{\mathbf{w}}_0(p,\omega)]^{T*}\bar{\mathbf{w}}_0(p,\omega) = S_I^{*}(p,\omega)[\mathbf{Z}(p,\omega)]^{*}[\mathbf{C}_{\mathrm{R}}(p,\omega)]^{*} \times [\Phi(p,\omega)]^{T*}\Phi(p,\omega)\mathbf{C}_{\mathrm{R}}^{T}(p,\omega)\mathbf{Z}^{T}(p,\omega)S_I(p,\omega). \quad (9)$$

We can recognize the spectrum of the combined excitation and instrument response $S_I^{*}(\omega)S_I(\omega)$. The propagation phase term $[\Phi(p,\omega)]^{T*}\Phi(p,\omega)$ will reduce to the identity in the far-field from any source, since the components are orthogonal and the phase cancels out between the two complex conjugate terms. We are then left with the far-field contribution,

$$[\mathbf{w}_0(p,\omega)]^{T*}\mathbf{w}_0(p,\omega) = [\mathbf{Z}(p,\omega)]^{*}[\mathbf{C}_{\mathrm{R}}(p,\omega)]^{*} \times \mathbf{C}_{\mathrm{R}}^{T}(p,\omega)\mathbf{Z}^{T}(p,\omega)[S_I^{*}(p,\omega)S_I(p,\omega)]. \quad (10)$$

We now can recognize the spectrum of the transmission term $[\mathbf{C}_{\mathrm{R}}(p,\omega)]^{*}\mathbf{C}_{\mathrm{R}}^{T}(p,\omega)$ modulated by external amplitude effects. Recognizing that the Fourier transform of a product produces a convolution in the time domain, we obtain

$$\mathcal{A}[\mathbf{w}_0(p,t)] = \mathcal{A}[S_I(p,t)] * \mathcal{A}[\mathbf{C}_{\mathrm{R}}^{T}(p,t)] * \hat{\mathbf{Z}}(p,t), \quad (11)$$

where we have written $\mathcal{A}[\ ]$ for the autocorrelogram. The last term $\hat{\mathbf{Z}}(p,t)$ in (11) summarizes the amplitude effects on the wavefield before it arrives at the base of the local structure. Whatever the nature of the propagation before energy arrives at the level z_J on its way to the surface, the first two terms on the right-hand side of (11) will be present, whereas $\hat{\mathbf{Z}}(p,t)$ will be variable. We see that the autocorrelation of the surface displacement at a particular station contains scaled information on the reflection response of the structure beneath the station including free surface reverberations, but this is convolved with the combined effects of excitation by distant sources and the instrumental response.

The actual ground motion will include a span of slownesses as indicated in eq. (1). When we consider stacks over multiple time intervals, we can expect some randomization of the external amplitude modulation term $\hat{\mathbf{Z}}$. The principal stacked autocorrelation response will be

$$\langle\mathcal{A}[\mathbf{w}_0(t)]\rangle \approx \langle\mathcal{A}[S_I(p,t)]\rangle * \langle\mathcal{A}[\mathbf{C}_{\mathrm{R}}(p,t)]\rangle, \quad (12)$$

where the stacking over time, indicated by the angle brackets, will bring in a wide range of slownesses and so stack over slowness as well.

When we concentrate attention on just the vertical component of ground motion, the dominant terms in $\langle\mathcal{A}[\mathbf{C}_{\mathrm{R}}(p,t)]\rangle$ will arise from *P* waves with some conversions for arrivals further away from the vertical. For the case of a single reflector, the timing of reflected arrivals varies with slowness, but is stationary for near vertical arrivals. Hence, we can expect that the stacked autocorrelogram will produce a somewhat diffuse representation of the reflection response, which will resemble that for *P* waves at vertical incidence since the conversions will also be suppressed. Because the most prominent components of the transmitted field will be inclined to the vertical, the tendency will be for a stacked reflection to occur slightly later than the expected time for vertical incidence. Selective filtering can reveal the reflection terms against the background of the instrumental autocorrelation, but only the strongest contrasts in material properties are likely to be identifiable.

The process of autocorrelation emphasizes the arrivals that have a systematic pattern of delays from an arrival at a station (Fig. 2). In the case of upward transmission through a simple crust, waves reflected back from the free surface such as Pp_mp will have the equivalent delay pattern to a simple reflection from the crust–mantle interface p_mp (Fig. 3). We can then think of the stacking process as enhancing such internal crustal reflections which are common to a wide class of incident waves.

3 DATA AND METHOD

We have constructed stacked autocorrelograms for 269 Australian broadband seismic stations from the recently enhanced permanent seismic network and from deployments of portable instruments. The time span of the records employed ranges from a few months to ∼4 yr. To ensure data quality, seismic records that contained

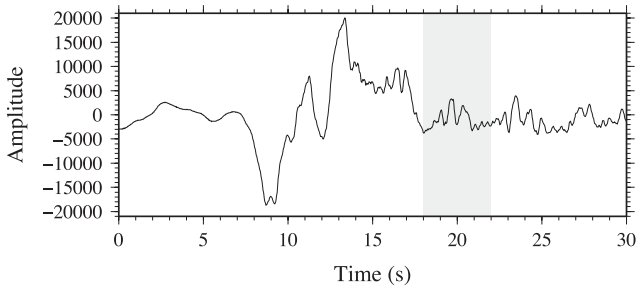

Figure 2. Observed vertical component at station NWAO of Mw 6.6 earthquake occurred near Papua & New Guinea on 2012 March 20 14:00:50. Grey area denotes start time from which reflections at lower crust and deeper, together with multiples, could be observed.

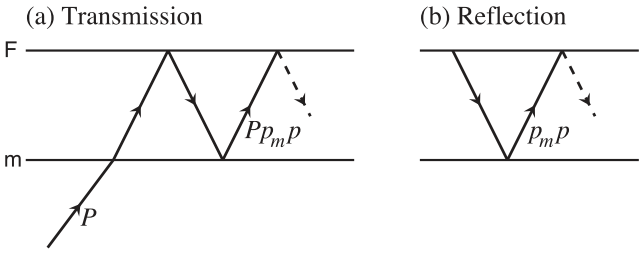

Figure 3. Equivalence of transmission and reflection results in the presence of a free surface (F) and reflector (m), the dashed path indicates further surface reflections.

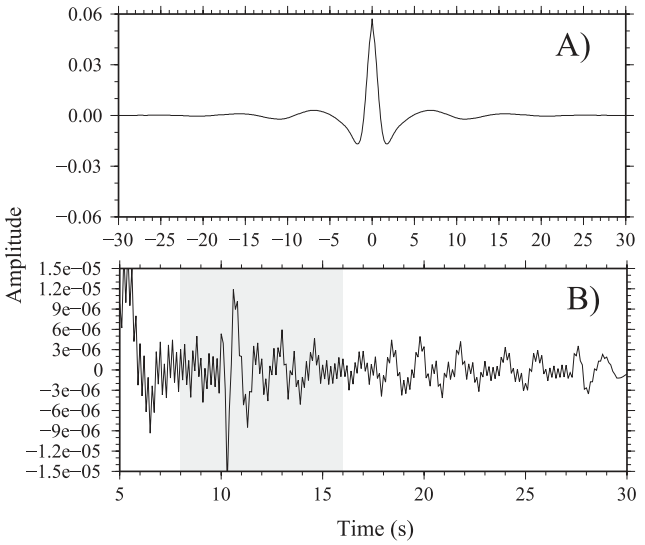

Figure 4. (a) Result of autocorrelation and stacking of continuous seismic waveforms recorded at station NWAO after removal of the instrumental response. (b) Enlargement of the stacked autocorrelogram for NWAO after removal of the instrument response (with high-pass filtering, corner 1 Hz), showing the presence of discrete arrivals associated with crustal reflections. The time window for reflections from the lower crust and Moho, 8–16 s time lag, is shaded.

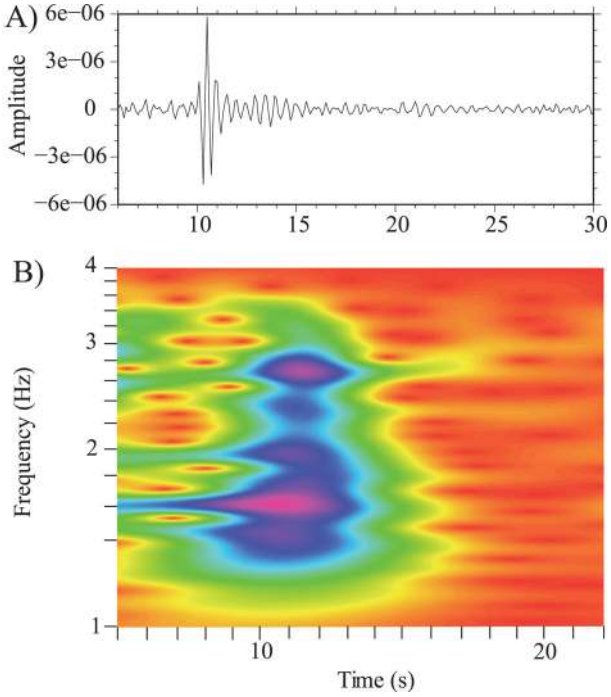

Figure 5. (a) The stacked autocorrelogram for NWAO after removal of the instrument response with bandpass filtering over the band 2–4 Hz. A distinctive pulse can be observed near 10 s linked to crustal reflection. (b) Dispersion analysis of autocorrelation function. There is no notable time shift for the pulse associated with reflected phases.

detected data gaps or spikes, related to instrumental problems, have been automatically rejected from further processing. The autocorrelations were calculated from the continuous records of the vertical components of ground motion at the seismic stations, employing 6 hr time windows. We have used a spectral procedure to calculate the autocorrelograms, as discussed in Appendix A. These autocorrelograms for the 6 hr windows were then stacked to enhance the coherent features and suppress the noise.

3.1 Stacked autocorrelograms for station NWAO

An example of the stacked autocorrelation results is shown in Fig. 4(a) for the station NWAO, in southwestern Australia. After applying data quality control, this autocorrelogram is based on one month of waveform records. For a permanent station such as NWAO, where the instrument characteristics are well known, we can remove the instrumental response and thereby take away part of the contribution that obscures the influence of structure near the station. The stacked autocorrelation trace shows a distinctive 'Mexican hat' shape arising dominantly from the excitation spectrum of the wavefield. The influence of instrumental response removal is very slight.

The concentration of the stacked autocorrelogram at zero time is a distinctive feature of the raw results for a station and tends to mask the reflection response near the station. The nature of the incident wavefield on the local structure will vary over time, but phases such as p_mp returned from crustal discontinuities (Fig. 3) will be a common feature with properties that vary slowly with the slowness of incident waves. In consequence, we expect them to stack, and so be detected in the autocorrelograms. In the light of the theoretical results above, we can regard the varied incident wavefields as generating time-varying virtual sources at the surface which illuminate the structure below, and give rise to reflected waves and their surface multiples. When we look in detail at the later portion of the stacked autocorrelograms at NWAO, we see a set of higher frequency arrivals superimposed on the longer period trend (Fig. 4b) in the time window where we would expect reflections from the lower crust and Moho (8–16 s time lag).

If we concentrate on the higher frequency content of the stacked autocorrelogram for station NWAO, we find in the time window for lower crustal reflections a distinctive pulse with a dominant frequency between ∼1.5 and ∼4 Hz (Fig. 5a). This arrival shows very clearly after bandpass filtering.

Frequency–time analysis of this part of the seismogram shows that the pulse near 10 s time lag shows no evident dispersion, which would be consistent with *P*-wave reflection from a crustal discontinuity (Fig. 5b).

3.2 Synthetic tests

In our study, continuous ground motion records at each seismic station have been processed without selection or rejection based on particular source information, an approach often seen in ambient noise seismic tomography. However, for purposes of synthetic test description, we can distinguish between informative signal parts such as body waves, arriving from earthquakes and everything else—noise caused by weather, sea waves or possible human activity (e.g. Rhie & Romanowicz 2004).

We have tested our ability to recover crustal reflections using the autocorrelation procedure by undertaking synthetic tests for a model with incident upgoing waves and a single prominent reflector (as in Fig. 3). We have used a single-layer crust with V_p 6 km s^{-1}, V_s 3.46 km s^{-1} and mantle velocities V_p 8.03 km s^{-1}, V_s 4.63 km s^{-1}. The depth of the crust mantle boundary (in metre) was variable and we show six test cases with a reflector at 5, 10, 15, 20, 25 and 50 km.

The response of the model was calculated using the reflection and transmission matrix approach of Kennett (1983) with a variety

of incident plane waves from the mantle. Seismic records with random number of seismic point sources, origin time, location (within slowness range 4.6–13 s deg^{-1}), focal mechanism and magnitude parameters were generated for every 24 hr and concatenated to simulate 1 yr of observations. In total 10 715 seismic sources have been generated that is similar to the average number of earthquakes reported by USGS for Sunda and Tonga-Kermadec subduction zones during an 1 yr period. This synthetic data were then subjected to the same processing steps as for the observations, and we find that we achieve definition of crustal reflections.

The results of the unfiltered stacked autocorrelation for the synthetic data, without noise, are shown in Fig. 6. When we consider synthetics without added noise, we get a very clear recovery of distinctive pulses that are associated with the reflection p_mp (Fig. 6a) and occur at the expected time for reflection from the major interface. What happens in the presence of noise? We have made a simulation with addition of white noise (Fox 1987) to the synthetic time segments, the level of noise was randomly specified with up to 15 per cent of signal allowed before the stacked autocorrelograms were constructed. The results show a strong resemblance in character to what we have seen for station NWAO (Fig. 4b). Visual comparison between both synthetic tests suggests that addition of white noise tends to broaden and distort the shape of recovered pulse. We have a noisy result, but the arrival corresponding to the reflected crustal phase is clearly visible at the same time lag (Fig. 6b).

3.3 Application to station network

The arrival time t was measured for largest observed amplitude on autocorrelogram for each station within the frequency band of 2–4 Hz. Although clear arrivals of reflected phases can often be observed within the frequency band of 1–4 Hz, the frequent presence of noise below ∼1.5 Hz tends to complicate the measurements. Therefore, a 2–4 Hz bandpass filter was chosen for consistent data processing for all stations. In case of multiple reflected arrivals, those that can be associated with deeper reflection have been taken as final measurement (see Appendix B). During selection of these final reflection time estimates, no *a priori* knowledge of structure was used to ensure the purity of experiment.

In total 269 stations have been processed yielding 223 measurements. Stations that have not been included in the final data set are those with (a) no clearly visible phase or (b) showing artefacts that could be attributed to poor data quality or instrumental problems. The resulting reflection times were converted to depths of p_mp reflection using a 6 km s^{-1} P wavespeed (V_p), a reasonable approximation for the complicated and diverse seismic structure of the Australian continent (M. Salmon, personal communication). Fig. 7 presents a map of Australia where the depth to the deepest prominent reflectors is depicted as isodepth curves. Examples of the filtered autocorrelograms for selected seismic stations distributed across the whole of the Australian continent are displayed in Appendix C.

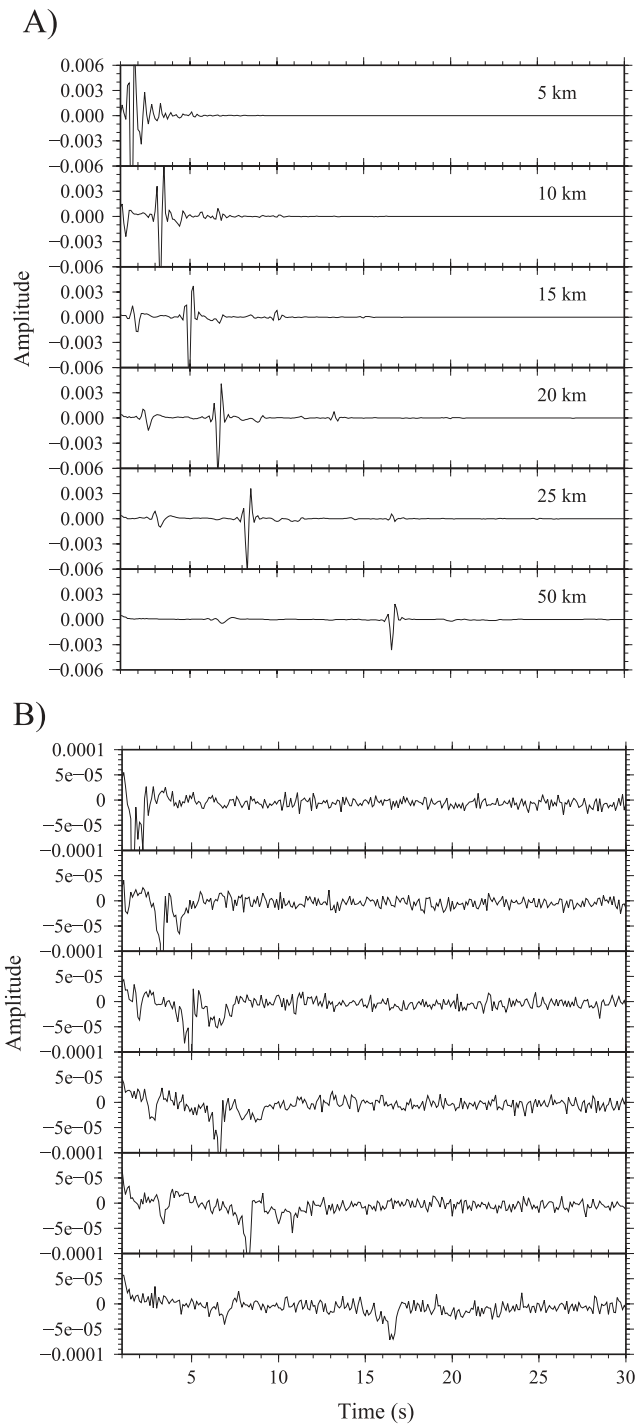

Figure 6. (a) Stacked autocorrelograms for synthetic seismic data with variable Moho depth. Moho depth in kilometres is marked on top right corner of each frame. (b) Unfiltered stacked autocorrelograms for synthetic seismic data with added white noise (see text for explanation).

4 DISCUSSION

The general pattern of isodepth curves of the deepest reflector, obtained in our studies (Fig. 7), shows some resemblance to the previously published results of Moho depth of Clitheroe *et al.* (2000) and somewhat less with that of Kennett *et al.* (2011). However, the recent results of Kennett *et al.* (2011) are derived from a much larger data set of diverse geophysical data, and are in good agreement with the gravity-based inversion for Moho depth by Aitken (2010). Kennett *et al.* (2011) point out the variability of the character of the Moho in both reflection and receiver function studies (their fig. 3). In many parts of the continent, there is a gradational transition between crustal and mantle wavespeeds that will not produce a prominent high-frequency reflection. In Fig. 8, we show an updated version of the Moho distribution (Salmon *et al.* 2012), including results from recent reflection profiling, which modify the Moho

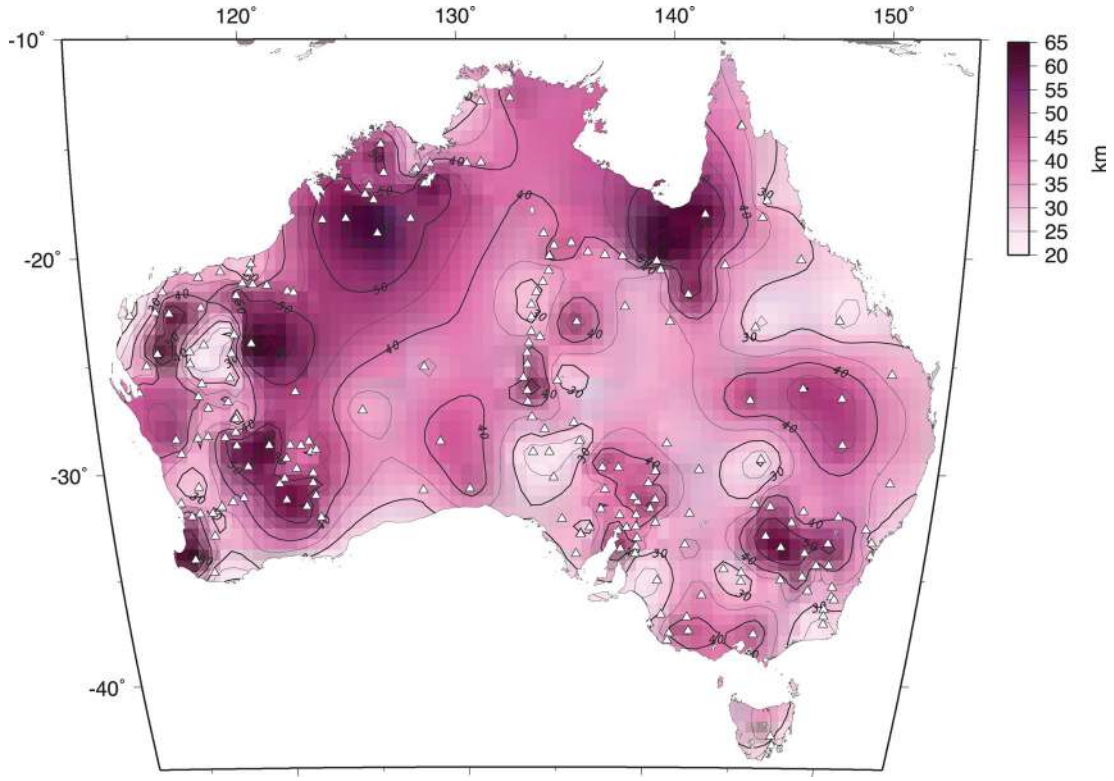

Figure 7. Depth to the deepest prominent reflector (in km) extracted from the stacked autocorrelograms for 223 stations, marked by triangles, across Australia.

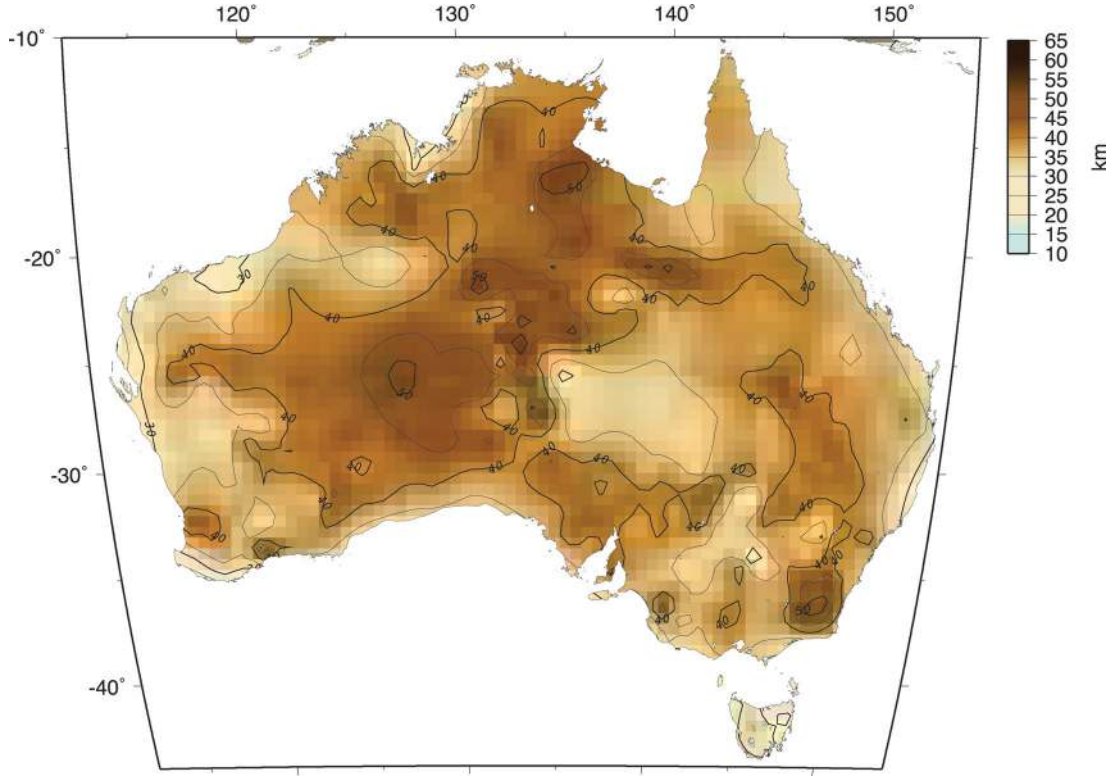

Figure 8. Depth to Moho (km), updated from Salmon *et al.* (2012), based on integration of many different types of seismological information.

distribution in southwestern Australia, with an improved match to the autocorrelation results.

In Fig. 9, we have created a profile across the Australian continent, choosing equally spaced stations located near 30° S, to illustrate the main features of the reflectors and associated autocorrelograms. We show the reflection responses for the various stations and the configuration of the choice of deepest reflector employed in Fig. 7. We see a clear pattern of late reflectors in Western Australia, tending

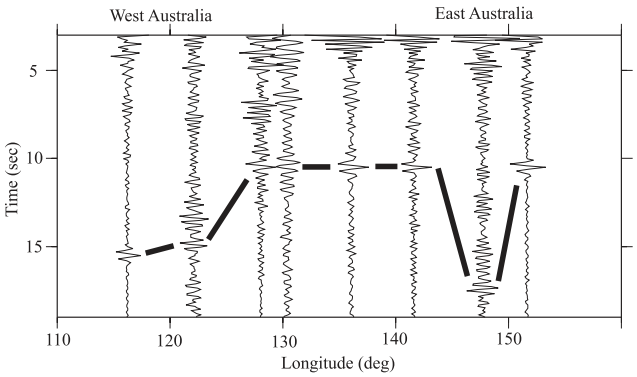

Figure 9. Profile across Australia showing the reflection traces from the autocorrelograms from stations close to the 30° parallel. Thick black lines indicate the location of the reflector selected for Fig. 7.

earlier in central Australia, with again an increase in reflection delay in the east. The very late reflection in Eastern Australia is not unexpected, there are observations of Moho depth to 50 km in this region; thus, the 17 s arrival is not likely to be an S reflection of the type reported by Tibuleac & Von Seggern (2012).

Although the general pattern of deep reflector distribution is in reasonable concordance with general tendency of Moho depths, there are differences in absolute values of the depth. An average seismic speed V_p of 6 km s^{-1} was adopted to convert observed times to the depth in our study. This velocity is the same as that used in Kennett *et al.* (2011) for depth conversion of Moho picks from reflection profiles, and provides good correspondence with results from receiver functions and refraction experiments in areas with multiple data sources.

As we have noted above, the time pick on the autocorrelogram can be expected to lie deeper than the true time to the reflector, because we are not able to apply any corrections for the variable slownesses of the components of the wavefield that are compounded into the stacked results. However, our results show not only areas with larger depths to the reflector than in the Moho map of Kennett *et al.* (2011), but also shallower depths as well (Fig. 8). In many parts of Australia, the transition from crust to mantle is gradational, and the Moho will then not be the strongest reflector for the high-frequency waves we have employed, rather we can get reflections from the lower crust, such as the top of the transitional zone. Fig. 10 shows the results of receiver function inversion for the station NWAO that indicate a sharp discontinuity at ∼29 km depth and gradual Moho (Clitheroe *et al.* 2000) at the depth of ∼40 km.

As a consequence, the autocorrelogram of NWAO station shows prominent pulse near 10 s (Fig. 5a), suggesting that it is detecting the stronger reflector in the lower crust rather than the gradual Moho discontinuity. In other cases where the crust is dominated by velocity gradients, there may be no sharp contrast to generate reflections. In such a case, we can get autocorrelograms where no clear pulse is visible, e.g. TL02 station located in Northern Australia (Fig. 11b). Little structure is detected in the receiver function inversion for the same station (Fig. 11a).

Theory and synthetic tests show that reflectors can be recovered using autocorrelation methods. Results of autocorrelation applied to continuous seismic records reveal a pattern of prominent reflectors similar to the Moho discontinuity configuration obtained in previous studies (e.g. Clitheroe *et al.* 2000; Kennett *et al.* 2011; Salmon *et al.* 2012). However, results obtained from autocorrelograms cannot always be directly interpreted as a Moho discontinuity due to the fact that the Moho can be gradual and, in consequence, will be

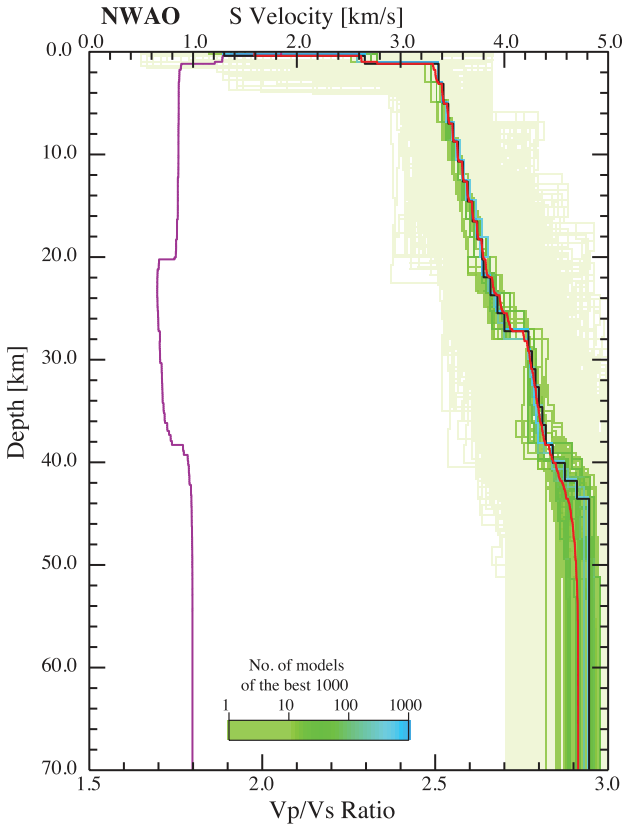

Figure 10. Results of the receiver function inversion at station NWAO (Clitheroe *et al.* 2000). Note the sharp discontinuity at ∼29 km and the gradual Moho at ∼40 km depth. The red line represents a weighted average of the best 100 models. The *Vp*/*Vs* ratio is indicated by the purple line.

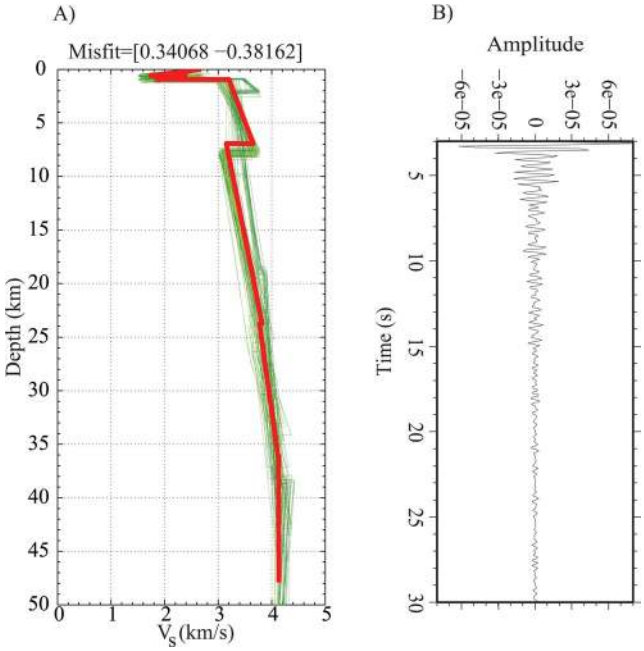

Figure 11. (a) Results of the receiver function inversion at station TL02 (Saygin 2007) and (b) autocorrelogram. Neither method shows the presence of reflectors in lower crust or upper mantle.

undetected by the autocorrelation method. Inclined discontinuities can also pose another challenge and will diminish the ability of the implicit stack in the autocorrelation approach to recover reflection signal. In the case of a strong but gradual change in seismic impedance, the upper, lower or both boundaries of a transition zone may be detected from autocorrelations, depending on the precise nature of the zone.

Analysis of autocorrelograms did not give us any hint that ability of reflector recovery is strongly linked to the amount of processed data. For example, the pulse at 10 s on the NWAO station correlogram, constructed from one month of data, is clearly visible, whereas station TL02 did not show any detectable reflectors after processing, in total, 1 yr of data. This observation suggests that reflector detection depends mainly on the structure below the seismic station rather than quantity of processed data, and even relatively short-term seismic deployments could be used for such studies.

Recent works show that body waves can be observed on two-station cross-correlations at few hundreds of kilometres (Zhan *et al.* 2010; Poli *et al.* 2012). In those cases as well the most important factor that permits to observe body waves seems to be the presence of simple crustal structure (e.g. small attenuation, large mean free path).

Our reconnaissance survey shows that we are able to extract reflection information from the stacked autocorrelograms of the continuous seismic records at stations located in the Australian continent. Where other sources of data exist, we can hope to improve the identification of arrivals. As we have seen (Fig. 7), there is general regional consistency in the reflections obtained from the stacked autocorrelograms, and this can also help us to extrapolate from regions of control and provide additional information from the new data source.

We have demonstrated that the stacked autocorrelograms provide additional information about the nature of the reflection response beneath a station. Care has to be taken in interpretation, but the results can already be exploited as an addition to receiver function analysis or other imaging techniques to analyse the presence of discontinuities in Earth structure. We hope to refine the procedures in further work.

ACKNOWLEDGMENTS

We would like to thank C. Collins and D. Burbidge for useful discussion and correction of the manuscript. K. Wapenaar and an anonymous reviewer made very valuable comments that greatly improved the manuscript. Generic Mapping Tools (Wessel and Smith 1998) were used in this study. This paper is published with the permission of the CEO, Geoscience Australia.

REFERENCES

Aitken, A.R.A., 2010. Moho geometry gravity inversion experiment (MoGGIE): a refined model of the Australian Moho and its tectonic and isostatic implications, *Earth planet. Sci. Lett.,* **297,** 71–83.

Betts, P.G., Giles, D., Lister, G.S. & Frick, L.R., 2002. Evolution of the Australian lithosphere, *Aust. J. Earth Sci.,* **49,** 661–692.

Claerbout, J., 1968. Synthesis of a layered medium from its acoustic transmission response, *Geophysics,* **33,** 264–269.

Clitheroe, G., Gudmundsson, O. & Kennett, B.L.N., 2000. The crustal thickness of Australia, *J. geophys. Res.,* **105**(B6), 13 697–13 713.

Collins, C.D.N., 1991. The nature of the crust-mantle boundary under Australia from seismic evidence, in *The Australian Lithosphere,* Vol. 17, pp. 67–80, ed. Drummond, B.J., Spec. Publ., Geol. Soc. Aust., Sydney.

Draganov, D., Wapenaar, K. & Thorbecke, J., 2006. Seismic interferometry: reconstructing the Earth's reflection response, *Geophysics,* **71,** SI61–SI70.

Fox, C.G., 1987. An inverse Fourier transform algorithm for generating random signals of a specified spectral form, *Comput. Geosci.,* **13**(4), 369–374.

Gouédard, P. *et al.*, 2008. Cross-correlation of random fields: mathematical approach and applications, *Geophys. Prospect.,* **56,** 375–393.

Frasier, C., 1970. Discrete time solution of plane P-SV waves in a plane layered medium, *Geophysics,* **35,** 197–219.

Kennett, B.L.N., 1983. *Seismic Wave Propagation in Stratified Media,* Cambridge University Press, Cambridge.

Kennett, B.L.N., 2001. *The Seismic Wavefield I - Introduction and Theoretical Development,* Cambridge University Press, Cambridge.

Kennett, B.L.N., 2002. *The Seismic Wavefield II - Interpretation of Seismograms on Regional and Global Scales,* Cambridge University Press, Cambridge.

Kennett, B.L.N. & Blewett, R.S., 2012. Lithospheric framework of Australia, *Episodes,* **35,** 9–22.

Kennett, B.L.N., Kerry, N.J. & Woodhouse, J.H., 1978. Symmetries in the reflection and transmission of elastic waves, *Geophys. J. R. astr. Soc.,* **52,** 215–230.

Kennett, B.L.N., Salmon, M. & Saygin, E. AusMoho Working Group, 2011. AusMoho: the variation of Moho depth in Australia, *Geophys. J. Int.,* **187,** 946–958.

Kunetz, A. & d'Erceville, E., 1962. Sur certaines propriétés d'une onde acoustique plane de compression dans une milieu stratifieé, *Ann. de Geophys.,* **18,** 351–359.

Poli, P., Pedersen, H.A. & Campillo, M. the POLENET/LAPNET Working Group, 2012. Emergence of body waves from cross-correlation of short period seismic noise, *Geophys. J. Int.,* **188,** 549—558. doi:10.1111/j.1365-246X.2011.05271.x.

Rhie, J. & Romanowicz, B., 2004. Excitation of Earth's continuous free oscillations by atmosphere–ocean–seafloor coupling, *Nature,* **431,** 552–556.

Roux, P., Sabra, K.G., Gerstoft, P., Kuperman, W.A. & Fehler, M.C., 2005. P-waves from cross-correlation of seismic noise, *Geophys. Res. Lett.,* **32**(L19303), doi:10.1029/2005GL023803.

Ruigrok, E., Campman, X. & Wapenaar, K., 2011. Extraction of P-wave reflections from microseisms, *Comptes Rendus Geosci.,* doi:10.1016/j.crte.2011.02.006.

Salmon, M., Kennett, B.L.N., Stern, T. & Aitken, A.R.A., 2012. The Moho in Australia and New Zealand, *Tectonophysics,* in press, doi: 10.1016/j.tecto.2012.07.009.

Saygin, E., 2007. Seismic receiver and noise correlation based studies in Australia, *PhD thesis,* Australian National University.

Saygin, E. & Kennett, B.L.N., 2010. Ambient noise tomography for the Australian Continent, *Tectonophysics,* **481,** 116–125.

Saygin, E. & Kennett, B.L.N., 2012. Crustal structure of Australia from ambient seismic noise tomography, *J. geophys. Res.,* **117** (B01304), doi:10.1029/2011JB008403.

Shapiro, N.M. & Campillo, M., 2004. Emergence of broadband Rayleigh waves from correlations of the ambient seismic noise, *Geophys. Res. Lett.,* **31** (L07614), doi:10.1029/2004GL019491.

Shapiro, N.M, Campillo, M., Stehly, L. & Ritzwoller, M.H., 2005. High-resolution surface-wave tomography from ambient seismic noise, *Science,* **307,** 1615–1618.

Tibuleac, I.M. & von Seggern, D., 2012. Crust–mantle boundary reflectors in Nevada from ambient seismic noise autocorrelations, *Geophys. J. Int.,* **189,** 493–500.

Ursin, B.J., 1983. Review of elastic and electromagnetic wave propagation in horizontally layered media, *Geophysics,* **48,** 1063–1081.

Wapenaar, K., Thorbecke, J. & Draganov, D., 2004. Relations between reflection and transmission responses of three-dimensional inhomogeneous media, *Geophys. J. Int.,* **156,** 179–194.

Wapenaar, K., van der Neut., J., Ruigrok, E., Draganov, D., Hunziker, J., Slob, E., Thorbecke, J. & Snieder, R., 2011. Seismic interferometry by crosscorrelation and by multidimensional

deconvolution: a systematic comparison, *Geophys. J. Int.,* **185,** 1335–1364.

Weaver, R.L. & Lobkis, O.I., 2001a. Ultrasonics without a source: thermal fluctuation correlation at MHz frequencies, *Phys. Rev. Lett.,* **87,** doi:10.1103/PhysRevLett.87.134301.

Weaver, R.L. & Lobkis, O.I., 2001b. On the emergence of the Green's function in the correlations of a diffuse field, *J. acoust. Soc. Am.,* **110,** 3011–3017.

Wessel, P. & Smith, W. H. F., 1998. New, improved version of the Generic Mapping Tools released, *EOS Trans. AGU,* **79,** 579.

Yoshizawa, K. & Kennett, B.L.N., 2004. Multi-mode surface wave tomography for the Australian region using a 3-stage approach incorporating finite frequency effects, *J. geophys. Res.,* **109**(B02310), doi:10.129/2002JB002254.

Zhan, Z., Ni, S., Helmberger, D.V. & Clayton, R.V., 2010. Retrieval of Moho-reflected shear wave arrivals from ambient seismic noise, *Geophys. J. Int.,* **182,** 408–420.

APPENDIX A: CONSTRUCTION OF AUTOCORRELOGRAMS

We use a regularized transfer function approach rather than a plain autocorrelation to mitigate effects caused by spectral holes and amplitude modulation due to instrument response. The frequency-domain representation of the autocorrelation given in (10) can be cast into the form of a spectral division, with a regularization factor using water level in the denominator:

$$\frac{[\bar{\mathbf{w}}_0(p,\omega)]^{T*}\bar{\mathbf{w}}_0(p,\omega)}{\max\left([\bar{\mathbf{w}}_0(p,\omega)]^{T*}\bar{\mathbf{w}}_0(p,\omega),\, \mathbf{c}\max\left([\bar{\mathbf{w}}_0(p,\omega)]^{T*}\bar{\mathbf{w}}_0(p,\omega)\right)\right)}, \tag{A1}$$

where $*$ denotes the complex conjugation and $(^T)$ is the matrix transpose. A water-level correction is applied to prevent strong amplitudes arising from small values in the denominator. This is achieved by assigning a preset maximum from the sample values in the denominator derived from the maximum of the autospectrum $\max\left([\bar{\mathbf{w}}_0(p,\omega)]^{T*}\bar{\mathbf{w}}_0(p,\omega)\right)$. The scaling factor $\mathbf{c}$ is determined *ad hoc* by trails over a range of values. We estimated that 1 per cent is optimum. This modified form of autocorrelation retains the phase characteristics of the standard autocorrelation but modifies the amplitude spectrum.

When we use (A1) for the theoretical representations of the crustal response (11), we obtain

$$\frac{\mathbf{Z}^*\mathbf{C}_{\mathrm{R}}^*\mathbf{C}_{\mathrm{R}}^T\mathbf{Z}^T[S_I^*S_I]}{\max\left(\mathbf{Z}^*\mathbf{C}_{\mathrm{R}}^*\mathbf{C}_{\mathrm{R}}^T\mathbf{Z}^T[S_I^*S_I],\, \mathbf{c}\max\left(\mathbf{Z}^*\mathbf{C}_{\mathrm{R}}^*\mathbf{C}_{\mathrm{R}}^T\mathbf{Z}^T[S_I^*S_I]\right)\right)}. \tag{A2}$$

Since stacking is carried out in the time domain, the amplitude modulation via $\mathbf{Z}$ will be reduced due to randomization, but the static terms associated with the crustal response $\mathbf{C}_{\mathrm{R}}$ and the instrument response S_{I} will remain. By introducing water-level regularization, the amplitude modulation $S_I^*S_I$ will be reduced, and yield robust results. Comparative example of standard autocorrelation and regularized autocorrelation for synthetic and observed seismic records is presented in Fig. A1. Synthetic data used for comparison are the same as that presented in Fig. 6.

Normalized autocorrelation used in our study shows better results, particularly on observed data (Fig. A1b). Autocorrelations applied to the synthetic data (Fig. A1a) gives additional visual hints about effect of regularization showing reduced presence of low-frequency signal on regularized autocorrelogram. Regularization enhances recovery of phases under study but could reduce low-frequency components of autocorrelograms, for examples those that could be associated with instrument response S_I.

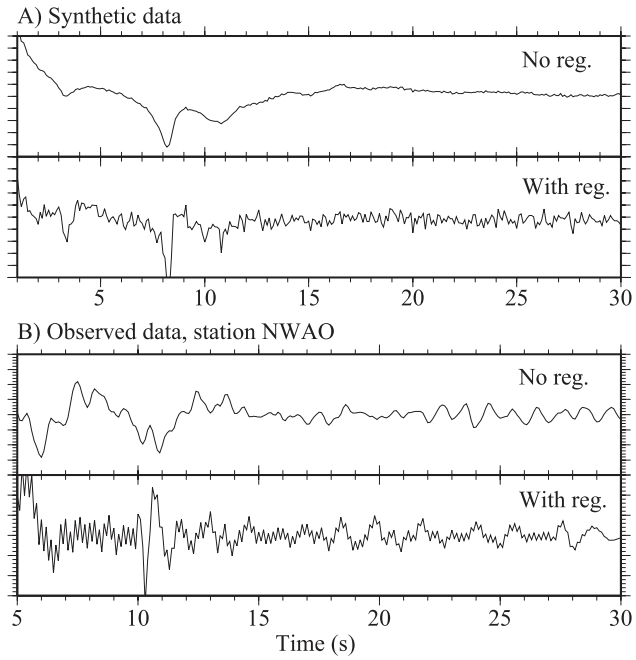

Figure A1. Comparison of standard and regularized autocorrelations for synthetic (set **A**) and observed (set **B**) data, respectively. Every set presents autocorrelograms normalized to unity where top is normal autocorrelation and bottom is normalized autocorrelation. Normalized autocorrelation recovers better reflected phases.

APPENDIX B: CHOICE OF REFLECTION PHASE

The reflection phase used to construct the map presented in Fig. 7 was based on the analysis of all clearly visible reflection phases (Fig. B1. Some stations, such as FORT located in South Australia, have multiple phase arrivals in the autocorrelations that make it difficult to choose which phase is most relevant for construction of the map of deep reflectors, since we may well have surface-generated multiples. For FORT, we can see three distinct groups of reflected phases, but no obvious surface multiples.

We conducted a blind process of final phase picking without taking into account *a priori* knowledge of Earth structure. In each case, the deepest phase, i.e. greatest time phase, was chosen (phase 3 in Fig. B1). Where the Moho is sharp, we could expect that this late picked phase might correspond to the Moho discontinuity. Earlier phases could be the Conrad discontinuity (phase 1) or a deep crustal discontinuity such as phase 2 (Fig. B1). Although Moho discontinuity could not be visible in certain circumstances,

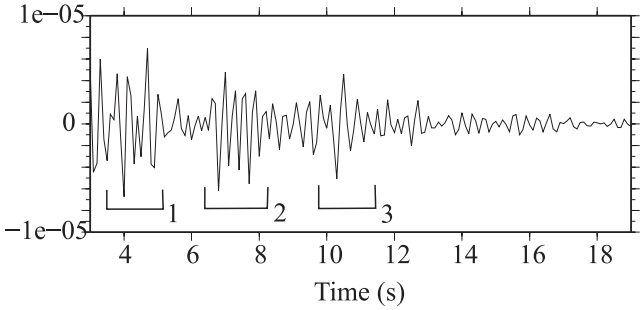

Figure B1. Autocorrelogram of station FORT. Three reflection phases are marked by corresponding numbers and highlighted by horizontal brackets.

our approach allows a consistent data processing scheme that aims to map the deepest detectable reflector regardless of its nature.

APPENDIX C: AUTOCORRELOGRAM EXAMPLE

A subset of 52 selected seismic stations homogeneously distributed across Australia (Fig. C1) is presented to provide an illustration of the results obtained from the filtered autocorrelograms. Grey rectangles in Figs C2 and C3 denote seismic phases identified as $p_m p$.

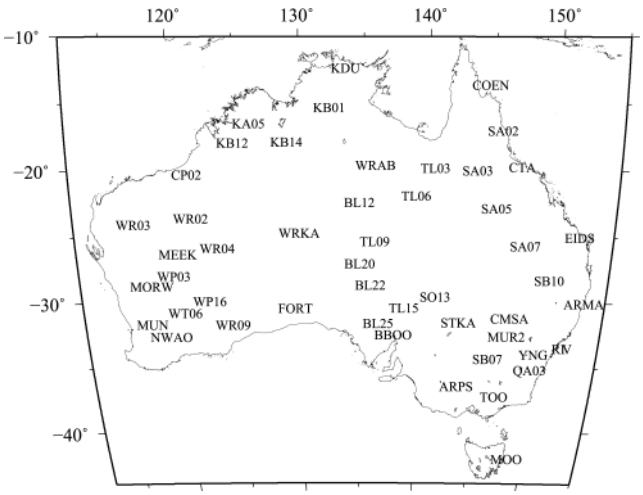

Figure C1. Location of seismic stations for subset of data presented below.

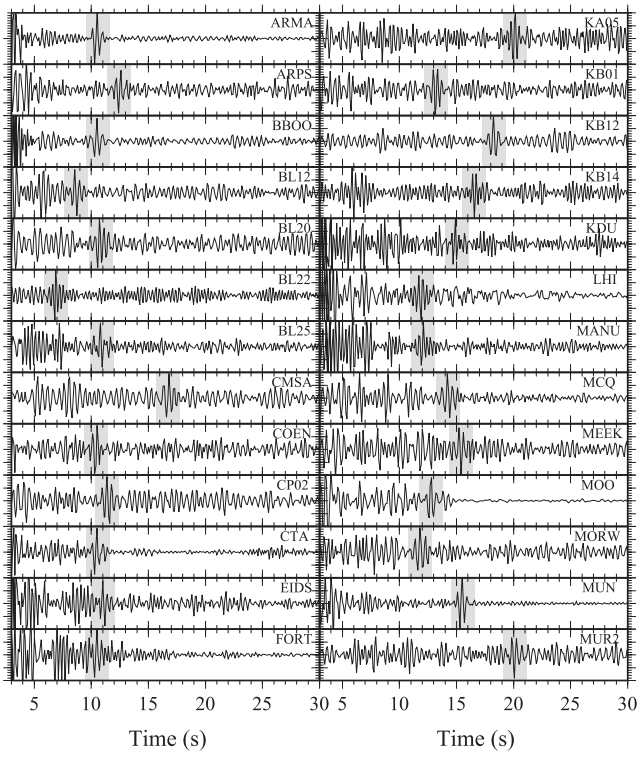

Figure C2. Example of autocorrelograms used in our study. See Fig. C1 for location. Grey rectangles denote seismic phases identified as $p_m p$.

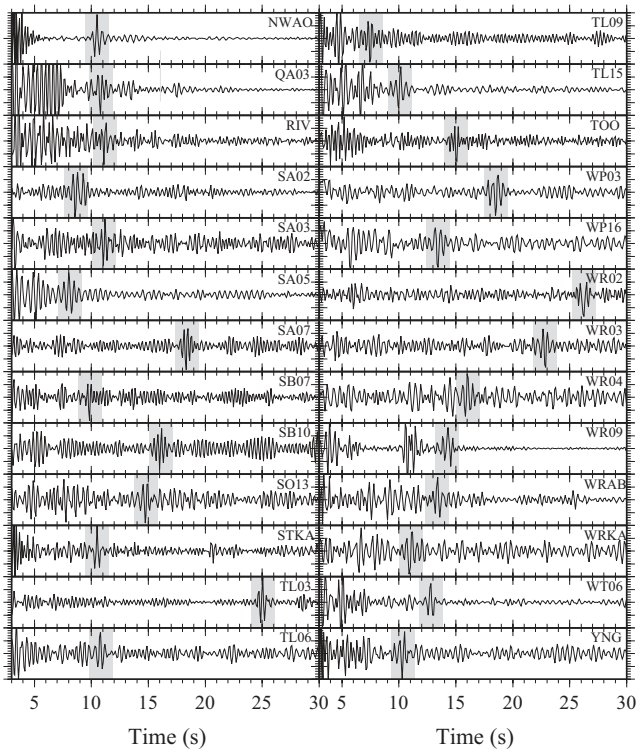

Figure C3. Same as Fig. C2.